Oscillation and Generation of Nonclassical States in Three-Photon Down-Conversion

Timo Felbinger, Stephan Schiller,* and Jürgen Mlynek
Fakultät für Physik, Universität Konstanz, D-78457 Konstanz, Germany
(Received 3 January 1997; revised manuscript received 14 July 1997)

The process of three-photon down-conversion $3\omega \rightarrow \omega + \omega + \omega$ in an optical cavity is analyzed theoretically. A classical feature of this system is a first-order transition of the fundamental mode above a threshold 3ω pump power. We calculate the properties of the intra- and extracavity states using analytical calculations and quantum trajectory simulations. A positive, non-Gaussian Wigner function exhibiting a threefold symmetry is found. Above threshold the Wigner function displays separate peaks among which tunneling occurs. [S0031-9007(97)04876-X]

PACS numbers: 42.50.Dv, 42.50.Lc, 42.65.St

The interaction between electromagnetic waves in nonlinear optical media plays a key role in quantum optics, as it provides a means of generating nontrivial quantum states of light. Preeminent among these are the squeezed states whose quantum uncertainty in one quadrature is less than that of a coherent state. Strongly squeezed states have been produced using second-order ($\chi^{(2)}$) nonlinear optical media, e.g., by two-photon down-conversion $2\omega \rightarrow \omega + \omega$ [1], as well as by self-phase modulation of high-power coherent light in third-order ($\chi^{(3)}$) media [2]. Except for the single-photon state, it has so far not been possible to generate experimentally other nonclassical states of light with the novel feature of non-Gaussian statistics.

This Letter reports the analysis of degenerate three-photon down–conversion (TD) $3\omega \rightarrow \omega + \omega + \omega$ in a $\chi^{(3)}$ medium as a possible source of a new class of quantum states of light. This process has been studied for running waves [3–5], but the small $\chi^{(3)}$ nonlinearities and limited laser powers available today rule out this configuration for generating continuous-wave optical fields. With this motivation, we discuss the resonant TD frequency conversion process shown in Fig. 1. The TD oscillator (TDO) is composed of an optical cavity resonant for the ω_1 and $\omega_3 = 3\omega_1$ waves, pumped by an injected coherent state of amplitude ε and frequency ω_3. Outcoupling of the two cavity modes occurs through the mirrors with loss rates γ_1 and γ_3. The modes interact via the Hamiltonian

$$\hat{H}^{(3)} = i\hbar\kappa^{(3)}(\hat{a}_1^{\dagger 3}\hat{a}_3 - \hat{a}_3^3\hat{a}_1^{\dagger}). \tag{1}$$

Both the interaction constant $\kappa^{(3)} \propto \chi^{(3)}$ and the amplitude ε of the incoupled field may be assumed to be real and positive. Three additional Kerr-like nonlinear interactions, which may be of the same order of magnitude as $\hat{H}^{(3)}$, have also to be taken into account:

$$\hat{H}^{(11)} = -\hbar\kappa^{(11)}\hat{a}_1^{\dagger 2}\hat{a}_1^2, \qquad \hat{H}^{(33)} = -\hbar\kappa^{(33)}\hat{a}_3^{\dagger 2}\hat{a}_3^2,$$
$$\hat{H}^{(13)} = -\hbar\kappa^{(13)}\hat{a}_1^{\dagger}\hat{a}_1\hat{a}_3^{\dagger}\hat{a}_3. \tag{2}$$

Under the influence of these terms, the cavity eigenfrequencies $\omega_{1,3}$ become intensity dependent; to compensate for this, we introduce detunings $\Delta_{1,3}$ relative to the eigenfrequencies $\omega_{1,3}^{(0)}$ at zero intensity: $\omega_{1,3} = \omega_{1,3}^{(0)} + \Delta_{1,3}$. To obtain the behavior of the TDO, we first derive the classical equations of motion and discuss their steady state solutions. The quantum properties are calculated using quantum trajectory simulations, including simulated homodyne detection and quantum state reconstruction. We finally give an analytical approximation derived from a perturbation expansion in the limit of a weak pump field.

Classical steady state solutions.—The classical equations of motion for the field amplitudes are

$$\dot{\alpha}_1 = 3\kappa^{(3)}\alpha_1^{*2}\alpha_3 + 2i\kappa^{(11)}\alpha_1^*\alpha_1^2 + i\kappa^{(13)}\alpha_1\alpha_3^*\alpha_3 - i\Delta_1\alpha_1 - \gamma_1\alpha_1, \tag{3}$$
$$\dot{\alpha}_3 = -\kappa^{(3)}\alpha_1^3 + 2i\kappa^{(33)}\alpha_3^*\alpha_3^2 + i\kappa^{(13)}\alpha_1^*\alpha_1\alpha_3 - i\Delta_3\alpha_3 - \gamma_3\alpha_3 + \varepsilon. \tag{4}$$

Here we are interested only in the stationary solutions, and we focus on the special case $\kappa^{(11)} = \kappa^{(13)} = \kappa^{(33)} = \Delta_1 = \Delta_3 = 0$ of no Kerr interactions and zero detunings. With nonvanishing Kerr interactions, the same stationary points (α_1, α_3) can then be realized by choosing $\Delta_1 = 2\kappa^{(11)}|\alpha_1|^2 + \kappa^{(13)}|\alpha_3|^2$ and $\Delta_3 = \kappa^{(13)}|\alpha_1|^2 + 2\kappa^{(33)}|\alpha_3|^2$. This choice is optimal in the sense that it will produce highest intracavity amplitudes for a given pump field.

The trivial solution $\alpha_1 \equiv 0$, $\alpha_3 = \varepsilon/\gamma_3$ is classically stable for all choices of the free parameters. This is a significant difference compared to the case of two-photon down-conversion, where the trivial solution is unstable above threshold. The stationary solutions with finite field α_1 lie on three curves; we give them in normalized form:

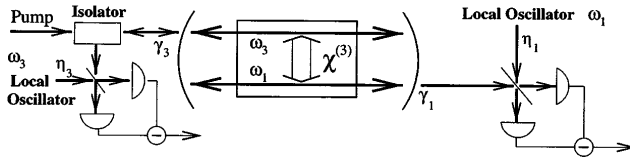

FIG. 1. Doubly resonant three-photon down-conversion in an optical cavity and balanced homodyne detectors for quantum state reconstruction.

 0031-9007/98/80(3)/492(4)$15.00

$$\alpha_1^{\mathrm{rel}} = |\alpha_1^{\mathrm{rel}}|\, e^{\frac{2\pi i}{3}n}, \qquad n \in \{0,1,2\},$$
$$\alpha_3^{\mathrm{rel}} = 1/|\alpha_1^{\mathrm{rel}}|, \qquad \varepsilon^{\mathrm{rel}} = |\alpha_1^{\mathrm{rel}}|^3/4 + 3|\alpha_1^{\mathrm{rel}}|/4, \tag{5}$$

where $\alpha_{1,3}^{\mathrm{rel}} := \alpha_{1,3}/\alpha_{1,3}^{\mathrm{th}}$, $\varepsilon^{\mathrm{rel}} := \varepsilon/\varepsilon^{\mathrm{th}}$, $|\alpha_1^{\mathrm{th}}| = (\gamma_1\gamma_3)^{\frac{1}{4}}/\sqrt{3\kappa^{(3)}}$, $\alpha_3^{\mathrm{th}} = \gamma_1^{\frac{3}{4}}/(\sqrt{3\kappa^{(3)}}\,\gamma_3^{\frac{1}{4}})$, and

$$\varepsilon^{\mathrm{th}} = \frac{4}{3\sqrt{3}}\,\frac{(\gamma_1\gamma_3)^{\frac{3}{4}}}{\sqrt{\kappa^{(3)}}}. \tag{6}$$

The set of stationary states of the fundamental mode has threefold symmetry in phase space; it is shown in Fig. 2. It can be seen that for any pump field amplitude ε above the threshold value $\varepsilon^{\mathrm{th}}$, there exist six stationary solutions with finite field α_1. Stability analysis reveals that the dashed branches represent unstable solutions; the solutions on the solid branches are stable, iff $\gamma_1 < \gamma_3$. The power conversion efficiency from the pump wave $3\omega_1$ to ω_1 reaches 100% at a pump power 3 times above threshold and decreases thereafter.

Quantum trajectory simulations.—We have performed quantum trajectory simulations using an algorithm similar to the one described in [6]. The evolution of the system is determined by a continuous Hamiltonian process, containing an anti-Hermitian term in addition to the nonlinear interaction, and one stochastic jump process per mode. We have generalized the stochastic process in [6] by simulating balanced homodyne detection instead of photon counting. For every mode j, this requires a stochastic process with three branches per time step τ,

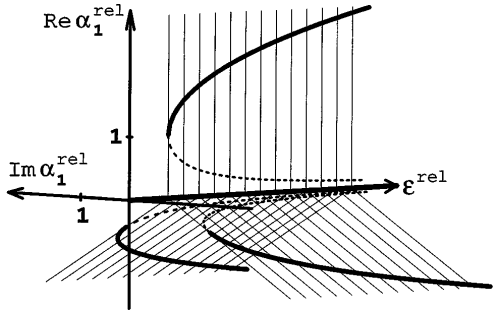

FIG. 2. Classical stationary solutions of the TDO as a function of pump field. The dashed branches represent unstable solutions.

$$|\Psi\rangle \mapsto \begin{cases} (\hat{a}_j + \eta_j)\,|\Psi\rangle, & p_{j,1} = \gamma_j\tau\,\dfrac{\langle\Psi|\,(\hat{a}_j^\dagger + \eta_j^*)\,(\hat{a}_j + \eta_j)\,|\Psi\rangle}{\langle\Psi\,|\,\Psi\rangle}, \\ (\hat{a}_j - \eta_j)\,|\Psi\rangle, & p_{j,2} = \gamma_j\tau\,\dfrac{\langle\Psi|\,(\hat{a}_j^\dagger - \eta_j^*)\,(\hat{a}_j - \eta_j)\,|\Psi\rangle}{\langle\Psi\,|\,\Psi\rangle}, \\ |\Psi\rangle, & p_{j,3} = 1 - p_{j,1} - p_{j,2}, \end{cases} \tag{7}$$

where η_j is the complex local oscillator amplitude. The first and second branch correspond to a click of the first and second detector, respectively, and the third branch describes the absence of a click during the time interval τ. The $p_{j,i}$ are the probabilities attributed to the branches.

In the simulations the two-mode state vector $|\Psi\rangle$ is expressed using a shifted Fock basis [7,8]. The classical solutions calculated above are a good choice, in most cases, for the origin (α_1, α_3) of the shifted basis. During the simulations, a new origin is chosen whenever the mean amplitudes differ from the current origin. This allows efficient representation of states containing more than 10 000 photons, as long as the state is sufficiently well localized in phase space, using typically only 32 or 64 basis vectors per mode [8].

The density matrix, and equivalently the Wigner function, is calculated by time averaging over a quantum trajectory $|\Psi(t)\rangle$. Figure 3 shows Wigner functions generated with parameters $\kappa^{(3)} = 0.15\gamma_1$, $\kappa^{(11)} = \kappa^{(13)} = \kappa^{(33)} = 0$, $\gamma_3 = 2\gamma_1$, for different pump field strengths ε below and above the threshold value $\varepsilon^{\mathrm{th}} = 3.34\gamma_1$. This threshold corresponds to a very low intracavity pump photon number of $N_3 = 1.25$. The emergence of peaks corresponding to the classically stable bright states (5) of the fundamental mode is obvious. Below threshold, the state of the system retains an interesting structure with threefold symmetry (a "star state"): its Wigner function is clearly non-Gaussian and not a minimum uncertainty state. Similar states have been described in [3–5] for a single-pass scheme, where negativities of the Wigner functions appear. Because our calculations refer to resonant modes and include losses, the resulting Wigner functions are non-negative. We show below that the emergence of this star state does not necessarily occur already below the threshold $\varepsilon^{\mathrm{th}}$ of parametric oscillation.

With nonzero Kerr interactions, cavity phase matching will no longer be fulfilled for all intensities; this causes curving of the Wigner function spikes; see Fig. 3.

Perturbation theory.—The parameters γ_1, γ_3, ε, and $\kappa^{(j)}$ appearing in the equations of motion all have the dimension of frequency and thus define independent time scales. Unfortunately, for experimentally accessible values, these time scales are expected to be very different, typically $\varepsilon \gg \gamma_j \gg \kappa^{(j)}$; quantum trajectory simulations in this regime are difficult. Furthermore, a figure of merit is desired to permit assessment of experimental feasibility of star states. To this end, we derive an analytical expression for the intracavity state by perturbation theory.

The approximation of the pump mode as a classical field, successful for the subthreshold states in two-photon down-conversion, fails for three-photon down-conversion [4,9–11]. This problem can be avoided by treating the pump mode quantum mechanically, which

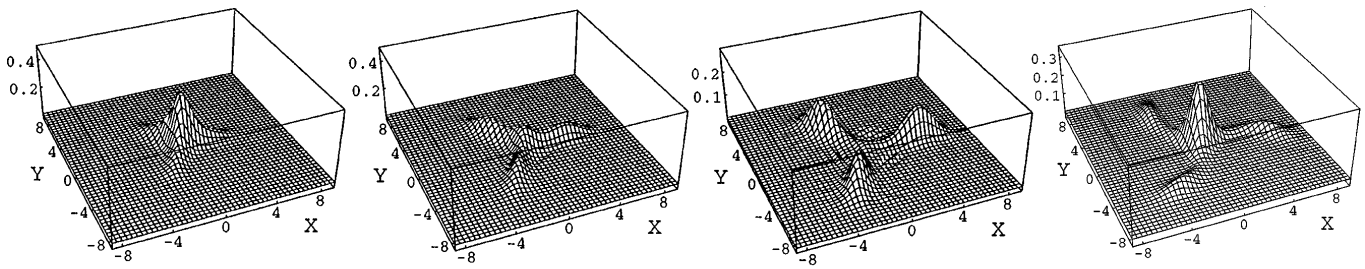

FIG. 3. (a)–(c) Wigner function of mode ω_1 inside the cavity as a function of pump field strength ε without Kerr interactions. The central peak disappears when ε is sufficiently far above threshold. (d) Intracavity Wigner function for a system with strong Kerr interactions: $\varepsilon/\varepsilon^{\rm th} = 1.21, s_3 = 0.175, \kappa^{(33)} = \kappa^{(11)} = \kappa^{(13)} = \kappa^{(3)} = 0.05\gamma_1, \gamma_3 = 2\gamma_1$.

has been shown for a single-pass scheme in [5]. For the intracavity problem, we find an analytical approximation for the steady state by perturbation expansion of the two-mode density operator, $\hat{\rho} = \hat{\rho}^{(0)} + \hat{\rho}^{(1)} + \hat{\rho}^{(2)} + \ldots$. The full Liouville equation for the two-mode system,

$$\frac{d}{dt}\hat{\rho} = -\frac{i}{\hbar}[\hat{H}, \hat{\rho}] + \mathcal{L}\hat{\rho} =: S\hat{\rho} + \mathcal{L}\hat{\rho}, \qquad (8)$$

must be split into an unperturbed part and a perturbation. Here S contains the nonlinear interactions $\hat{H}^{(3)}$, $\hat{H}^{(11)}$, $\hat{H}^{(13)}$, and $\hat{H}^{(33)}$, as well as the coupling to the pump field, and $\mathcal{L}$ is the loss operator. For the unperturbed part, we choose the modified loss operator $\mathcal{U}$,

$$\begin{aligned}\mathcal{U}\hat{\rho} := {} & \gamma_1(2\hat{a}_1\hat{\rho}\hat{a}_1^\dagger - \hat{a}_1^\dagger\hat{a}_1\hat{\rho} - \hat{\rho}\hat{a}_1^\dagger\hat{a}_1) \\ & + \gamma_3(2\hat{b}_3\hat{\rho}\hat{b}_3^\dagger - \hat{b}_3^\dagger\hat{b}_3\hat{\rho} - \hat{\rho}\hat{b}_3^\dagger\hat{b}_3), \end{aligned} \qquad (9)$$

where $\hat{b}_3 := \hat{a}_3 - (\varepsilon/\gamma_3)$. All remaining terms of the Liouville operator are taken to be the perturbation $\mathcal{P}$: $\mathcal{P} := S + \mathcal{L} - \mathcal{U}$. The zeroth order contribution to $\hat{\rho}$ is a product of coherent states with amplitudes equal to the classical subthreshold solution, $\hat{\rho}^{(0)} = |0, \varepsilon/\gamma_3\rangle\langle 0, \varepsilon/\gamma_3|$, which is an exact stationary solution of the unperturbed equation of motion, i.e., $\mathcal{U}\hat{\rho}^{(0)} = 0$. Perturbation corrections to the stationary solution can then be computed iteratively as

$$\hat{\rho}^{(n+1)} = -\mathcal{U}^{-1}\mathcal{P}\hat{\rho}^{(n)}. \qquad (11)$$

The inverse map $\mathcal{U}^{-1}$ exists for trace-free operators like $\mathcal{P}\hat{\rho}^{(n)}$; it becomes unique by demanding that all corrections $\hat{\rho}^{(n)}$, $n \geq 1$, must also be trace free. The first nonvanishing corrections on the main diagonal of the reduced density matrix $\hat{\rho}'$ of mode ω_1 in Fock basis, i.e., the first prediction of a finite population of Fock states higher than zero, occur in second order; in this order, the nonzero elements are

$$\begin{aligned} \rho'_{00} &= 1 - \frac{11}{3}s_3^2, \qquad \rho'_{11} = 2s_3^2, \qquad \rho'_{22} = s_3^2, \\ \rho'_{33} &= \frac{2}{3}s_3^2, \qquad \rho'_{30} = \sqrt{\frac{2}{3}}\, s_3(1 + 2is_{11}) = \rho'^{*}_{03}, \\ \rho'_{60} &= \frac{2}{3}\sqrt{5}\, s_3^2 = \rho'_{06}, \end{aligned} \qquad (12)$$

with $s_{11} := \kappa^{(11)}/\gamma_1$ and $s_3 := \kappa^{(3)}\varepsilon/(\gamma_1\gamma_3)$. s_3 can be interpreted as a figure of merit: In order to observe a state of the fundamental mode significantly different from vacuum, s_3 must be comparable to 1. Carrying the perturbation expansion up to eighth order, we found very good agreement of the Wigner functions below threshold with the numerical results.

Extracavity field.—The quantum state emitted by the cavity is of central interest. It can be reconstructed from the probability distributions of a full set of generalized quadrature components $X_\theta, \theta \in [0, \pi]$ [12,13]; the click rates of the simulated homodyne detection system provide us with this information.

We concentrate first on the two orthogonal quadrature components $X \equiv X_0$ and $Y \equiv X_{\pi/2}$. The phase θ_j of each η_j in the stochastic process (7) is switched by $\pi/2$ each time step, resulting in a quasisimultaneous measurement of X and Y on mode j. This procedure keeps the state vector well localized in phase space as can be seen in Fig. 4. The system spends most of its time close to one of the classical solutions, with "tunneling" events [14] occurring at random intervals. This is qualitatively similar to the conventional $\chi^{(2)}$ parametric oscillator [8].

"Bright" states corresponding to finite amplitude solutions on the solid branches in Fig. 2 with photon numbers of the order of 10^4 can also be simulated; although there are four classically stable points, tunneling between peaks corresponding to different classical solutions is extremely unlikely at high amplitude, so single peaks can

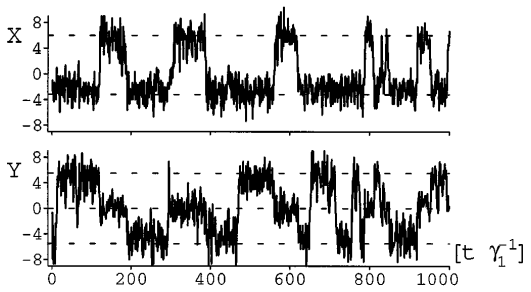

FIG. 4. Typical quasisimultaneous quantum trajectories of fundamental mode extracavity quadratures, derived from the homodyne detection rates. Dashed lines represent classical steady state solutions.

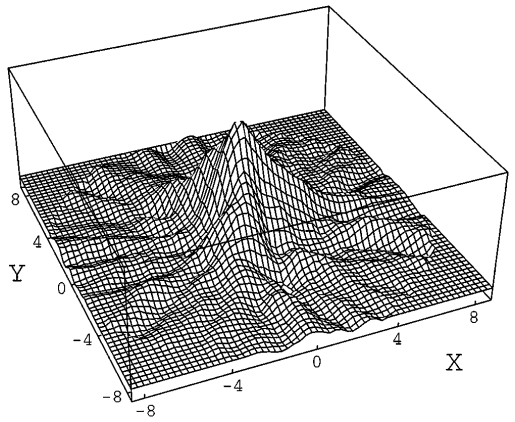

FIG. 5. Subthreshold extracavity Wigner function reconstructed from the simulated homodyne detection rates, corresponding to the intracavity state shown in Fig. 3(a).

be realized. In this regime, the states of both fundamental mode and pump mode are approximately Gaussian squeezed states, with the mean amplitudes in good agreement with the classical solution. The degree of squeezing can be derived in the usual way from the linearized classical equations of motion [8,15].

Figure 5 shows the Wigner function of a subthreshold state, reconstructed by inverse Radon transformation from 150 samples of X_θ for each of 36 different θ values distributed evenly over the interval $[0; \pi]$. Every sample was obtained by summing detector clicks for five cavity lifetimes, thus simulating a detector bandwidth narrow relative to the cavity linewidth, as is done experimentally [13]. We have assumed absence of intracavity losses.

The steady state of the emitted field can be given in analytical form, in the limit of small s_3,

$$|\Psi\rangle \approx |0\rangle + \frac{is_3\gamma_1}{c}\left(\frac{L}{2\pi}\right)^{\frac{3}{2}} \int_{-\frac{\pi}{L}}^{\frac{\pi}{L}} dk_a\, dk_b\, dk_c \times \left(\frac{1}{k_a + k_b + k_c} - i\pi\delta(k_a + k_b + k_c)\right) \times \prod_{j\in\{a,b,c\}} \frac{t_1 b^\dagger_{K_1+k_j}}{1 - r_1 e^{ik_j L}} |0\rangle ,$$

where $\hat{b}_k^\dagger$ is the creation operator for a free photon with wave vector k, L is the cavity roundtrip length, K_1 is the wave vector of the intracavity mode $\hat{a}_1$, $t_1 = \sqrt{2L\gamma_1/c}$ is the transmittivity, and $r_1 = \sqrt{1 - t_1^2}$ is the reflectivity of the cavity mirror. The state contains a superposition of photon triplets with frequencies $\omega_j = c(K_1 + k_j)$ lying mostly within one cavity bandwidth γ_1 around the cavity eigenfrequency ω_1. It is not normalizable but the predicted intensity of the emitted field agrees with (12).

In conclusion, our calculations show that the TDO has two quite independent thresholds. Parametric oscillation can occur above the threshold pump power $P^{\text{th}} = |\varepsilon^{\text{th}}|^2\hbar\omega_3/(2\gamma_3)$. Assuming a Gaussian-mode cavity and a typical value $\chi^{(3)} = 6 \times 10^{-23}\ \text{m}^2\,\text{V}^{-2}$ for the third-order susceptibility, we find that P^{th} depends only on the cavity losses $T_1 = t_1^2$ and $T_3 = t_3^2$ of the modes ω_1 and ω_3 per roundtrip: $P^{\text{th}} \approx (10^6\ \text{W})\sqrt{T_1^3 T_3}$. For realistic losses, P^{th} can be of the order of 100 W. On the other hand, generation of a distinct star state of the fundamental mode requires a figure of merit $s_3 \approx 1$. For the corresponding pump power $P_\star$, we find the relation

$$P_\star/P^{\text{th}} \approx P^{\text{th}}/\hbar\omega_3\gamma_1 , \tag{13}$$

which is typically much greater than 1. This situation is in contrast to the case of two-photon down-conversion, where substantial squeezing of the fundamental mode occurs already below the theshold of parametric oscillation [16]. We conclude that an experimental realization of TDO appears to be achievable in the near future, while generation of nonclassical states via three-photon down-conversion requires novel nonlinear media.

We thank G. Breitenbach, H. Hansen, and Ch. Hettich for clarifying discussions on experimental feasibility and the reconstruction of the extracavity Wigner function, as well as C. Savage, A. Bandilla, and G. Drobný for helpful suggestions.

Note added.—After review of the manuscript we became aware of Bajer's work [17] in which the classical properties of the TDO are analyzed.

*Electronic address:
http://quantum-optics.physik.uni-konstanz.de

[1] E. S. Polzik *et al.*, Phys. Rev. Lett. **68**, 3020 (1992); C. Kim and P. Kumar, Phys. Rev. Lett. **73**, 1605 (1994); G. Breitenbach *et al.*, J. Opt. Soc. Am. B **12**, 2304 (1995).
[2] K. Bergman *et al.*, Opt. Lett. **19**, 290 (1994).
[3] S. L. Braunstein and R. I. McLachlan, Phys. Rev. A **35**, 1659 (1987).
[4] P. V. Elyutin and D. N. Klyshko, Phys. Lett. A **149**, 241 (1990).
[5] K. Banaszek and P. L. Knight, Phys. Rev. A **55**, 2368 (1997).
[6] K. Mølmer *et al.*, J. Opt. Soc. Am. **10**, 524 (1992).
[7] R. Schack *et al.*, J. Phys. A **28**, 5401 (1995).
[8] T. Felbinger, Diploma thesis, Universität Konstanz, 1996.
[9] R. A. Fisher *et al.*, Phys. Rev. D **29**, 1107 (1984).
[10] M. Hillery, Phys. Rev. A **42**, 498 (1990).
[11] G. Drobný and I. Jex, Phys. Rev. A **45**, 1816 (1992).
[12] K. Vogel and H. Risken, Phys. Rev. A **40**, 2847 (1989); D. T. Smithey *et al.*, Phys. Rev. Lett. **70**, 1244 (1993).
[13] G. Breitenbach *et al.*, Nature (London) **387**, 471 (1997).
[14] This is not quantum tunneling in the strict sense: there is no energetically forbidden potential barrier separating the peaks.
[15] H. J. Carmichael, in *Coherence and Quantum Optics VII*, edited by J. Eberly *et al.* (Plenum, New York, 1996), p. 177; *An Open Systems Approach to Quantum Optics* (Springer, New York, 1993).
[16] For the $\chi^{(2)}$-OPO, the expansion parameter equivalent to s_3 is $s_2 = \kappa^{(2)}\,\varepsilon/\gamma_1\,\gamma_2$, where $s_2 = 1$ is the threshold for parametric oscillation.
[17] J. Bajer, J. Mod. Opt. **38**, 1085 (1991).